Computational Investigation of the Mechanisms of Particle Separation and "Fish-Hook" Phenomenon in Hydrocyclones

B. Wang
Laboratory for Simulation and Modelling of Particulate Systems, School of Materials Science and Engineering, The University of New South Wales, Sydney, NSW 2052, Australia

Key Laboratory of Western China's Environmental Systems (Ministry of Education), College of Earth and Environmental Sciences, Lanzhou University, Lanzhou 730000, P.R. China

A. B. Yu
Laboratory for Simulation and Modelling of Particulate Systems, School of Materials Science and Engineering, The University of New South Wales, Sydney, NSW 2052, Australia

DOI 10.1002/aic.12114
Published online November 12, 2009 in Wiley InterScience (www.interscience.wiley.com).

The motion of solid particles and the "fish-hook" phenomenon in an industrial classifying hydrocyclone of body diameter 355 mm is studied by a computational fluid dynamics model. In the model, the turbulent flow of gas and liquid is modeled using the Reynolds Stress Model, and the interface between the liquid and air core is modeled using the volume of fluid multiphase model. The outcomes are then applied in the simulation of particle flow described by the stochastic Lagrangian model. The results are analyzed in terms of velocity and force field in the cyclone. It is shown that the pressure gradient force plays an important role in particle separation, and it balances the centrifugal force on particles in the radial direction in hydrocyclones. As particle size decreases, the effect of drag force whose direction varies increases sharply. As a result, particles have an apparent fluctuating velocity. Some particles pass the locus of zero vertical velocity (LZVV) and join the upward flow and have a certain moving orbit. The moving orbit of particles in the upward flow becomes wider as their size decreases. When the size is below a critical value, the moving orbit is even beyond the LZVV. Some fine particles would recircuit between the downward and upward flows, resulting in a relatively high separation efficiency and the "fish-hook" effect. Numerical experiments were also extended to study the effects of cyclone size and liquid viscosity. The results suggest that the mechanisms identified are valid, although they are quantitatively different. © 2009 American Institute of Chemical Engineers *AIChE J,* 56: 1703–1715, 2010

Keywords: hydrocyclone, multiphase flow, computational fluid dynamics, separation mechanism, fish-hook effect

Introduction

A hydrocyclone is a device to classify or separate particles in a liquid suspension based on the densities or sizes of particles. It has two exits on the axis: a small one at the bottom (underflow or reject) and a large one at the top (overflow or

Correspondence concerning this article should be addressed to A. B. Yu at a.yu@unsw.edu.au.

accept). The underflow is generally the denser or thicker fraction, while the overflow is the lighter or more fluid fraction. Hydrocyclones are widely used in industry, particularly in mineral and chemical processing, because of their simplicity in design, high capacity, low maintenance and operational cost, and small physical size.[1,2] Normally, the so called partition curve is used to quantify and compare the performance of classification in hydrocyclones, which shows the fraction of a material of a specific size in the feed to a classifier that reports to the coarse product stream (underflow). In general, the partition curve decreases monotonically with particle size and asymptotes to a given value called the "bypass."[3] However, it is sometimes observed that the recovery of fine particles in a hydrocyclone underflow increases with the decrease of particle size beyond a critical particle size. This phenomenon is generally termed as the "fish-hook" effect in the literature.[4]

Different hypothesis have been proposed to explain the fish-hook effect. Plitt[5] pointed out that this phenomenon was due to a certain portion of feed solids being bypassed to the underflow, which was assumed to be directly proportional to water recovery. However, Frachon and Cilliers[3] found that the recovery of water from the underflow was significantly lower than either the lowest point of the partition curve at the bottom of the fish-hook or the value of the bypass. They thought that the fish-hook phenomenon was possibly due to a boundary layer flow which moved small particles directly to the underflow stream. Flintoff et al.[6] considered the fish-hook effect occurred due to poor experimental procedures and measurements. Nageswararao[7] further suggested that the fish-hook effect was a random and sporadic occurrence caused by the imprecision of measurement of the selective value and it did not affect the hydrocyclone performance prediction. On the other hand, Majumder et al.[4] believed the occurrence of the fish-hook phenomenon in hydrocyclones dealing with fine particles was not random but definite, which was confirmed by Roldán-Villasana et al.[8] who analyzed the partition curves with rigorous population balance reconciliation. Finch[9] and Neesse et al.[10] pointed out that the reason was related to the entrainment of fine particles in polydisperse suspensions. Kraipech et al.[11] and Majumder et al.[12] further gave an explanation that fine particles were dragged by the wakes generated behind larger particles. The different views indicate that the mechanism governing the fish-hook phenomenon is very complicated and likely multifaced. There is a need to conduct a systematic study to better understand the phenomena.

The fish-hook effect should be related to the flow of particles and the mechanism of particle separation in a hydrocyclone, which is however not well understood. So far, most of the papers about the mechanisms[13–17] stated that particles move relative to the fluid with respect to the balance of outward centrifugal and inward drag forces acting upon particles in the radial direction. The coarser or heavier particles with relatively high centrifugal force move toward the wall and flow downward to the apex of the cone. The fluid phase which carries the smaller or lighter particles with relatively high inward drag force, approaches the apex and reverses in the axial direction spiraling upward and escapes through the vortex finder. According to this hypothesis, however, two questions are raised. First, why does the drag force on particles point to the center? As the direction of the drag force mainly depends on the relative velocity between fluid and particle, the fluid must have a very high inward velocity in hydrocyclones. But many studies show the radial velocity of fluid is small and even does not point to the center.[18–20] The other question is if the drag force can reach that high level to balance the high centrifugal force the magnitude of which can be hundred times that of the gravity. These two questions can not be explained satisfactorily from the work reported.[13–17] It seems that there are not only the drag force and centrifugal force acting on particles, but also another force playing an important role in hydrocyclones.

To understand the mechanisms behind the fish-hook effect and the separation behavior of hydrocyclones, it is essential to investigate the motion of particles. Until now, many studies have been focused on the liquid field in hydrocyclones.[18,19,21,22] Few researchers studied the motion of solid particles. Recently, Wang et al.[23] published an experimental investigation using a high-speed motion analyzer (HSMA) system to track the trajectories of solid particles. However, details about the dynamics is still lacking in their work.

This article presents a numerical study of the particle flow and fish-hook phenomenon in hydrocyclones. The dynamics of solid particles is analyzed using the stochastic Lagrangian model. The results are found to be useful in understanding the mechanisms about the fish-hook effect and the particle separation behavior of hydrocyclones.

Mathematical Model

Model description

The multiphase flow in a hydrocyclone is quite complicated, and different treatments may have to be used for different phases. In this work, the fluid flow is modeled as turbulent, described by the Reynolds stress model (RSM), the interface between the liquid and air core is modeled by the volume of fluid (VOF) model, and the outcomes of these process are then applied in the simulation of particle flow described by the stochastic Lagrangian model. The RSM used has been proven to be an appropriate model to describe the anisotropic turbulence of cyclone flow although it is computationally more expensive than other unresolved-eddy turbulence models.[18] On the other hand, the VOF-free surface model can describe the interface between the liquid and air core in a hydrocyclone. In the VOF model used, gas and liquid, the two fluids considered in this work, share a single set of momentum equations, and the volume fraction of each of the fluids is tracked throughout the computational domain. The interface between the air core and the liquid in a hydrocyclone is then determined as a transient process. Details about the use of the CFD models can be found elsewhere.[18] Below the model to describe the flow of particles is briefly described because it is directly related to the discussion in this work.

The motion of a particle of mass m, density ρ_p and particle size d_p is described by the stochastic Lagrangian multiphase flow model. The liquid drag force and pressure gradient force on particles are calculated in a Lagrangian reference frame, given by

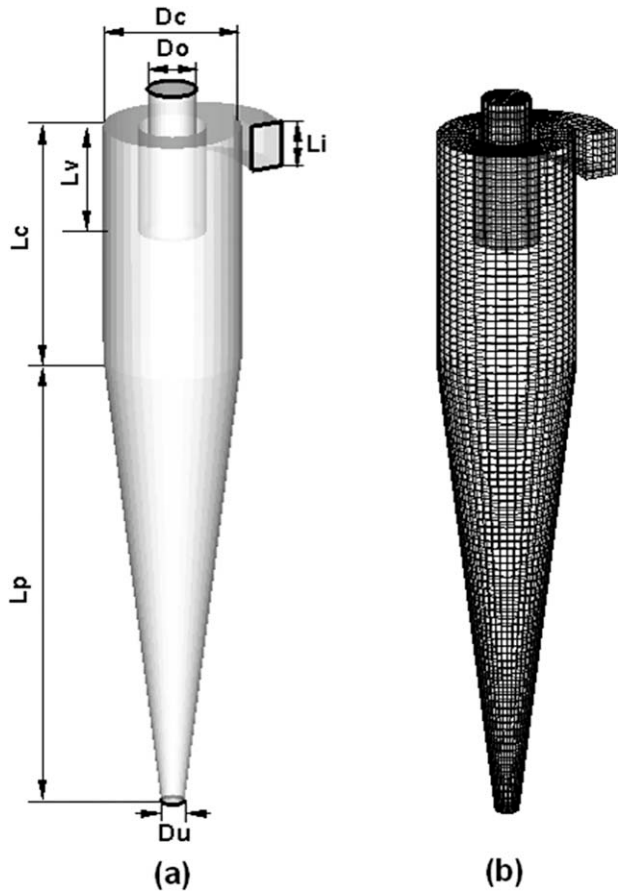

Figure 1. Schematic (a) and grid (b) representation of the original hydrocyclone considered.

$$\frac{d\vec{u}_p}{dt} = F_D(\vec{u} - \vec{u}_p) - \frac{\nabla p}{\rho_p} + \vec{g} \tag{1}$$

where F_D is the drag coefficient, given by

$$F_D = \frac{18\mu}{d_p^2 \rho_p} C_D \frac{Re_p}{24} \tag{2}$$

where $\vec{u}_p$ is the particle velocity and $\vec{u}$ is the velocity of the fluid phase. Re_p is the relative Reynolds number.

In the stochastic tracking, the turbulent dispersion of particles is predicted by integrating the trajectory equations for individual particles, using the instantaneous fluid velocity, $\overline{u} + u'$, along the particle path during the integration. The values of u' that prevail during the lifetime of the turbulent eddy are sampled by assuming that they obey a Gaussian probability distribution:

$$u' = \zeta\sqrt{\overline{u'^2}} \tag{3}$$

where ζ is a normally distributed random number. As the kinetic energy k of turbulence is known at each point in the flow, the values of the RMS fluctuating components can be obtained (assuming isotropic) as:

$$\sqrt{\overline{u'^2}} = \sqrt{\overline{v'^2}} = \sqrt{\overline{w'^2}} = \sqrt{2k/3} \tag{4}$$

Particle–eddy interaction time and dimension should not be larger than the lifetime and size of a random eddy. It is noted that use of Eq. 4 implies that turbulence influences the construction of the eddy velocity isotropically. As pointed out by Kallio and Reeks,[24] this assumption is inappropriate when particles move in the strongly anisotropic turbulent buffer region near a wall.

In this work, all the numerical simulations were conducted using the Fluent CFD software package (v6.0). The second-order upwinding and the SIMPLE pressure-velocity coupling algorithm were used. The convergence strategy used the unsteady solver and the time step was chosen as 10^{-4} to 10^{-2} s. Trial tests show that the results are not sensitive to the time step in this range.

Simulation conditions

Figure 1a shows a common classifying hydrocyclone designed for coal preparation, which consists of eight main geometrical parameters: diameter of the cylindrical body (D_c), length of inlet (of square shape) (L_i), diameter of vortex finder (D_o), diameter of spigot (D_u), length of cylindrical part (L_c), length of vortex finder (L_v), thickness of vortex finder (D_v), and length of conical part (L_p). Table 1 lists the values of the geometrical parameters in this work. The pressure at the two outlets (vortex finder and spigot) is 101,325 Pa, and the inlet water velocity and particle velocity are both 4.085 m/s (flow rate = 150 m^3/hr). Coal particles with a density of 1437 kg/m^3 are injected at the inlet. The liquid is assumed to be homogeneous. Unless otherwise stated, its viscosity is set to 1.003 cP. A ''velocity inlet'' boundary condition is used at the cyclone inlet, and both outlets use the ''pressure-outlet'' condition. Because the volume percentage of solid phase is less than 10%, it is reasonable to ignore the effect of the solid phase on the liquid phase and the interaction between particles.

Figure 1b shows the computational domain of the original model. The computational domain is divided by unstructured hexahedron grids. In the vicinity of the walls and vortex finder, the grid is refined. Trial numerical results demonstrate that the solution is independent of the mesh size used.

Model validation

It is necessary to validate the mathematical model before its application for numerical experiments. This is done by comparing the predicted and measured experimental flow fields including the tangential and axial velocity distributions at different axial locations in our recent work.[18] The measurements are taken from the work of Hsieh[20] involving the

Table 1. Geometry of the Hydrocyclone Considered

Parameter	Symbol	Dimension (mm)
Diameter of the body	D_c	355
Side length of inlet	L_i	120 × 85
Diameter of vortex finder	D_o	125
Thickness of vortex finder	D_v	25
Diameter of spigot	D_u	60
Length of cylindrical part	L_c	630
Length of vortex finder	L_v	285
Length of conical part	L_p	1205

use of laser doppler velocimetry (LDV). Moreover, the comparison between the experimental and numerical results has also been made for the performance in the hydrocyclone, such as pressure drop, volume split ratio, and separation efficiency. The experimental results agree reasonably well with the calculated ones. The errors are less than 10%.

Results and Discussion

General fluid flow pattern

The flow field of fluid is important because it largely decides the movements of solid particles. Figure 2 shows some representative snapshots of the simulated flow field of liquid flow. There is an air core (here defined as the regions

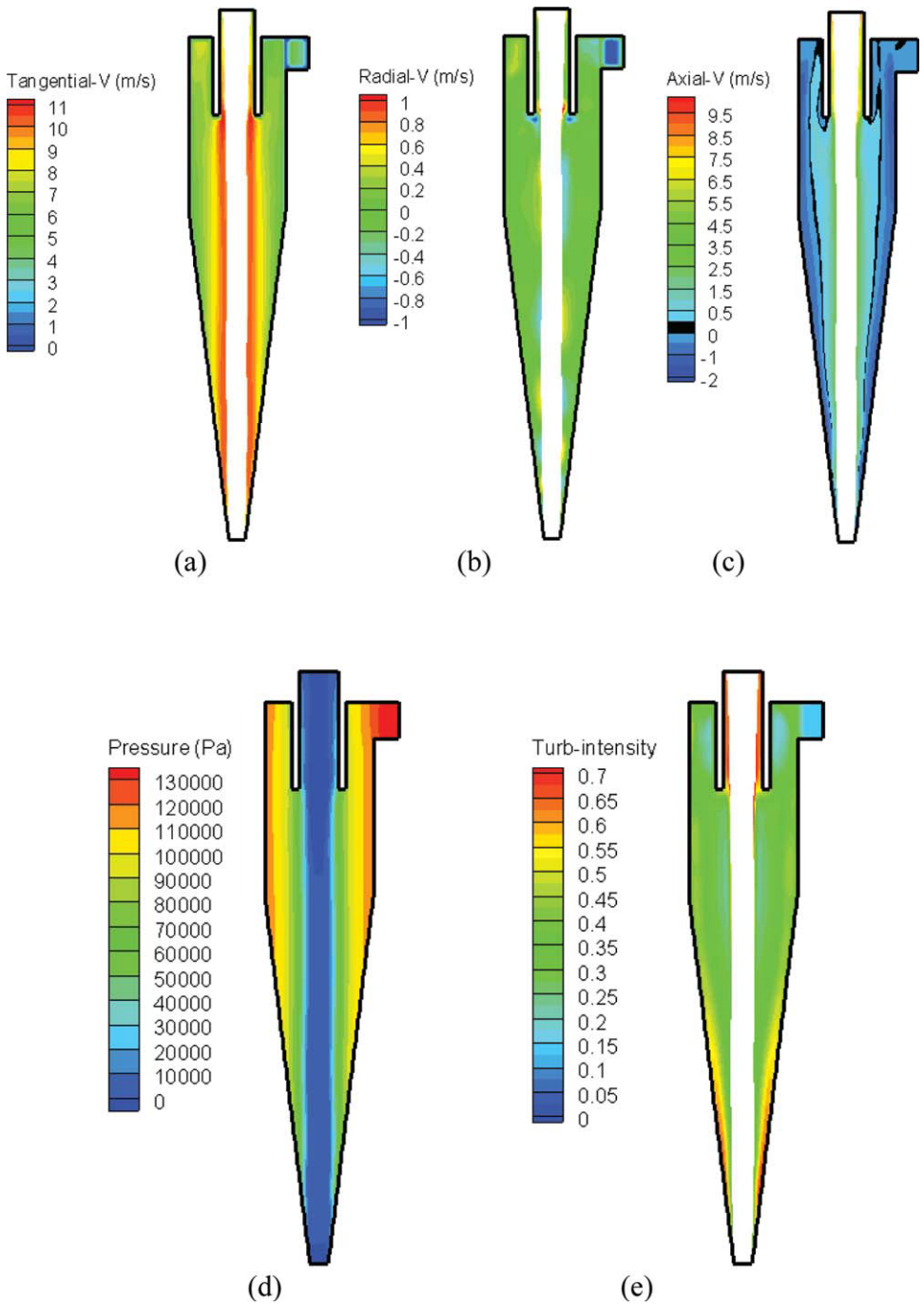

Figure 2. Spatial distributions of: (a) tangential velocities, (b) radial velocities, (c) axial velocities, (d) static pressure, and (e) turbulence intensity in the model hydrocyclone.

[Color figure can be viewed in the online issue, which is available at www.interscience.wiley.com.]

with volume fraction of air larger than 0.9) located around the central axis of the hydrocyclone. Figure 2a shows that the tangential velocity increases from the outer wall to the center of the hydrocyclone and reaches its peak value at the region close to the air core. As shown in Figure 2b, the distribution of radial velocity is like a helical twisted cylinder. The axis of the forced vortex does not coincide with the geometrical axis of the cyclone, and being curved rather than straight. The black line in Figure 2c represents the dividing line of axial velocity between the upward and downward flow, which was named the locus of zero vertical velocity (LZVV).[1] It can be seen that fluid flows downward along the cyclone wall and flows upward in the regions close to air core. Figure 2d shows that the static pressure decreases radially from the wall to the center, and a low pressure zone is formed in the center. The pressure gradient is the largest along the radial direction. Figure 2e shows the turbulence intensity distribution in the hydrocyclone. In the outer downward flow, the turbulence intensity remains uniform in the cylindrical part and increases with the decrease of height in the conical part. In the inner upward flow, the intensity is smaller and more uniform compared with the downward flow, except for the flow in the vortex finder.

Partition curve and fish-hook phenomenon

Figure 3 shows the calculated separation recovery to underflow as a function of coal particle size. The partition curve presents a fish-hook shape. The tendency of the curve can be divided into four regions, as reported by some researchers.[4,17]

In Region A, the separation efficiency attains to 100%, which means all particles located in the region report to the underflow. In Region B, the efficiency increases with increasing particle size; this trend is the same as the classification function in a hydrocyclone. In Region C, the efficiency decreases with particle size before reaching a fish-hook minimum, the dip point. In Region D, the particle size is smaller than the critical point, the particle diameter over which the fish-hook effect occurs, and the separation efficiency increases with the increase of particle size. However, it is noted that such fine particles in the region is normally not considered in the evaluation of the cyclone performance. Their motion may be governed by other micro forces, such as the van der Waals force and Brownian force.[25] Therefore, the behaviors of particles in this region are not included in this work. The following nomenclature has been proposed to differentiate the shape of a "fish-hook" curve.

- Cut point: the particle size where the separation recovery is 50%.
- Dip point: the particle size where the recovery is minimum.
- Critical point: the critical particle size from which the recovery of relatively coarse particle in the underflow starts decreasing.
- Depth: the difference between the recoveries of respective particles at the critical point and at the dip point.

To investigate the particle flow and fish-hook effect in the hydrocyclone, five typical particles of different sizes shown in red throughout the curve are selected for detailed analysis of their trajectories, positions, and forces in the hydrocyclone. They are of 105 μm with 100% separation efficiency located in Region A, 46 μm with 50% separation efficiency (cut point), 31 μm with 17% separation efficiency in Region B, 16 μm with 5% separation efficiency (dip point) and 1 μm particle with 36% separation efficiency (critical point). The results are discussed in the following subsessions.

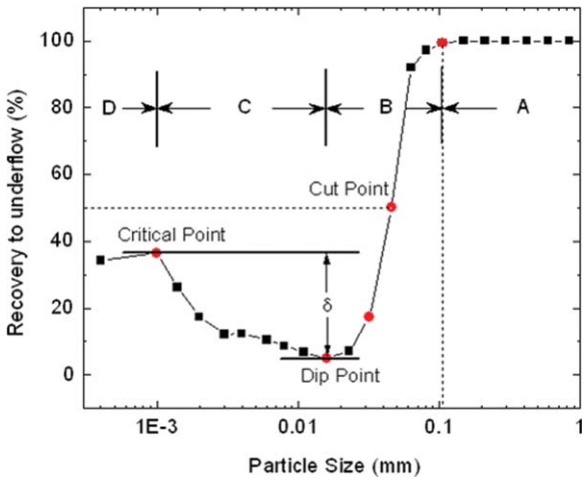

Figure 3. The partition curve of the hydrocyclone.

[Color figure can be viewed in the online issue, which is available at www.interscience.wiley.com.]

In a hydrocyclone, the motion of a particle is stochastic to a large extent. However, the motion of many particles can be characterized statistically. In this work, the results from the dynamic analysis of an individual particle which is injected from the center of inlet and the spatial distribution of particles in the cyclone are used to represents the stochastic and statistical characteristics, respectively. To be statistically meaningful, 45,000 particles are simulated for each considered size. This consideration applies to all the results used below.

Flow of particles in Region A

Figure 4 shows the trajectories and the forces acting on a 105 μm coal particle. In the figure, the three columns correspond to the tangential, radial, and axial directions, respectively, and the five rows represent distance, velocity, drag force per mass, pressure gradient force per mass and total force per mass respectively. In the tangential direction, anticlockwise is positive and clockwise is negative. In the radial direction, outward is positive and inward is negative, and the center of cyclone is the zero point. In the axial direction, upward is positive and downward is negative, and the roof of the hydrocyclone is the zero point. The treatments apply to the other figures in the article.

It can be seen from the first row in Figure 4 that the particle goes down along the wall of the cyclone and report to the underflow according to the distance distribution. The residence time of such a particle is about 1.5 s. It falls into the conical part from cylindrical part at 0.5 s. The second row shows the velocity distribution in the three directions. The tangential velocity of the particle initially increases rapidly in the inlet section, and then decreases in the cylindrical part. In the cone, the swirling velocity goes up, and has an

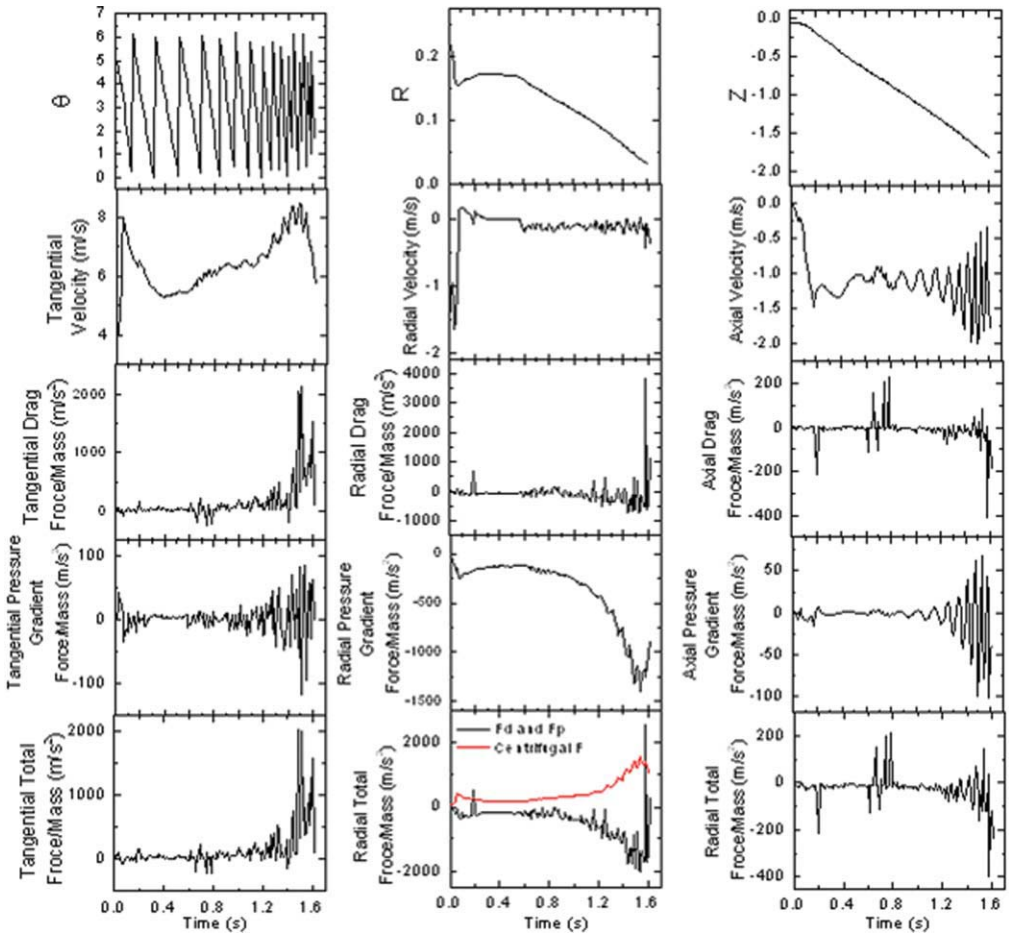

Figure 4. Dynamic result of a representative 105 μm particle (columns: tangential, radial, and axial directions; rows: position, velocity, drag force, pressure gradient force, and total force).

[Color figure can be viewed in the online issue, which is available at www.interscience.wiley.com.]

apparent drop before the particle escapes from the spigot. The radial velocity is zero at the cylinder and keeps a certain negative value in the conical part, which indicates the particle moves downward along the wall of the cyclone. The third row shows the fluid drag force per mass in the three directions. There is a sudden change of the drag force when the particle is near the spigot because of the local high turbulence intensity, shown in the Figure 2e. It is noted that the magnitude of the drag force in the radial direction is much higher than that in the other two directions. The pressure gradient force per mass shown in the fourth row has a very high negative value in the radial direction comparing with other two, which pushes the particle toward the center. Moreover, as the height decreases, the effect of the pressure gradient force becomes stronger. The fifth row shows the total force per mass in the three directions. In the tangential and axial directions, the curve of the total force is similar to the drag force, which means the drag force plays a dominant role in these two directions. In the radial direction, however, the pressure gradient force is the most important. As a result, the particle is pushed in the inward direction. On the other hand, the centrifugal force ($= v_t^2/r$, where v_t is the tangential velocity of particle located at an orbit radius r) shown in red color has a reverse direction and pushes the particle toward the wall of the hydrocyclone. For this particle, the centrifugal force is higher than the inward total force. So, finally the particle reports to the underflow.

Figure 5a shows a snapshot of the spatial distribution of 105 μm particles in the hydrocyclone when the fluid and particle flow remains steady. In the figure, the red and blue lines present the LZVV and the boundary of air core respectively. The red and blue points mean the particles have upward and downward velocities, respectively. It can be seen that all particles stay in the downward flow and has a downward velocity. None of particles has a reverse motion to the upward flow, which corresponds to the results that all particles in this region reports to the underflow as shown in Figure 3.

Flow of particles at cut point and in Region B

Particles at the cut point have a size 46 μm as shown in Figure 3. As shown in Figure 6, the flow characteristic of this 46 μm particle is similar to the 105 μm particle. From the Z position, this particle is discharged from underflow and the residence time is about 1.6 s. It is noted that the drag force has a strong fluctuation when the time is 1.2 s. At that time, the axial position of the particle is in the middle of the

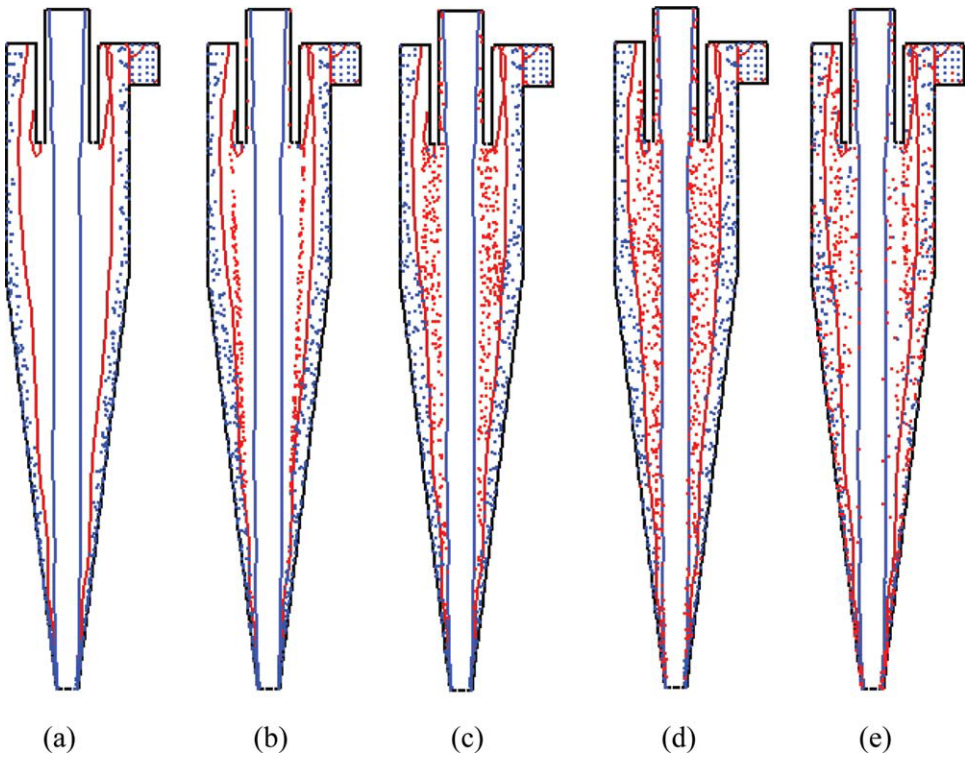

Figure 5. Spatial distribution of particles of different sizes: (a) 105 μm, (b) 46 μm, (c) 31 μm, (d) 16 μm, and (e) 1 μm (red line: LZVV; blue line: boundary of air core; blue point: particles with downward velocity; red point: particles with upward velocity).

[Color figure can be viewed in the online issue, which is available at www.interscience.wiley.com.]

conical part with high turbulence intensity. Correspondingly, the stochastic characteristic becomes significant due to the high drag force. As a result, some particles could be pushed to the upward flow in that region and report to the overflow finally.

Figure 5b shows some 46 μm particles are discharged from underflow and the others turn around to the upward flow and exit from the overflow. It is interesting that the region where some particles turn around from the downward flow to the upward flow is from the middle of the conical part to the spigot. In this region, the turbulence intensity is high (Figure 2e), which generates a high drag force with nondirectional characteristic. Some particles are pushed to the inner flow stochastically. Once the particles go into the upward flow where the turbulence intensity is low, the pressure gradient force and the centrifugal force are balanced keeping the particles in the upward flow with a certain moving orbit. Moreover, this distribution indicates that the movement of particles of the cut size is not along the LZVV, which does not agree with the equilibrium orbit theory.[1,2] The equilibrium orbit theory assumes that particles of a given size will reach an equilibrium radial orbit position inside the hydrocyclone where their outward terminal settling velocity is equal to the inward radial velocity of the liquid. Accordingly to this theory, the cut size is defined as the particle size whose equilibrium orbit is coincident with the locus of zero vertical velocity of the fluid. Such a particle will have equal chance to escape the hydrocyclone either through the underflow or through the overflow.

Changing particle size gives different behavior. As an example, a particle of 31 μm is selected for discussion. It can be seen from Figure 7 (the first row) that the 31 μm particle goes down initially, then up and finally is discharged from the overflow. The total residence time is about 3 s. At 0.4 s, the particle goes into the cone from the cylinder and then turns around from the downward to upward flow at 1.7 s. The tangential velocity of the particle is high and the radial velocity fluctuates apparently around zero value when the particle is in the upward flow. Compared with coarser particles as discussed earlier, the pressure gradient force does not change much quantitatively. Some small changes are due to the position of the particle. On the other hand, the drag force has a significant fluctuation, particularly in the radial direction. It would give the particle more opportunities to cross the LZVV and result in a low efficiency to the underflow. When time is 0.8 s, the particle moves to the junction between the cylindrical and conical parts where the radial drag force has a sudden change due to the high turbulence intensity, which means the separation could occur from the junction to the spigot.

Figure 5c shows the spatial distribution of 31 μm particle. Many particles turn around from the junction between the cylindrical and conical parts to the bottom of the cyclone and report to the vortex finder. Some upward particles are collected by the so called short circuit flows[18] under the bottom of vortex finder. It is noted that the moving orbit of 31 μm particles in the upward flow becomes wider than that of 46 μm particles. There are here two reasons. First, the

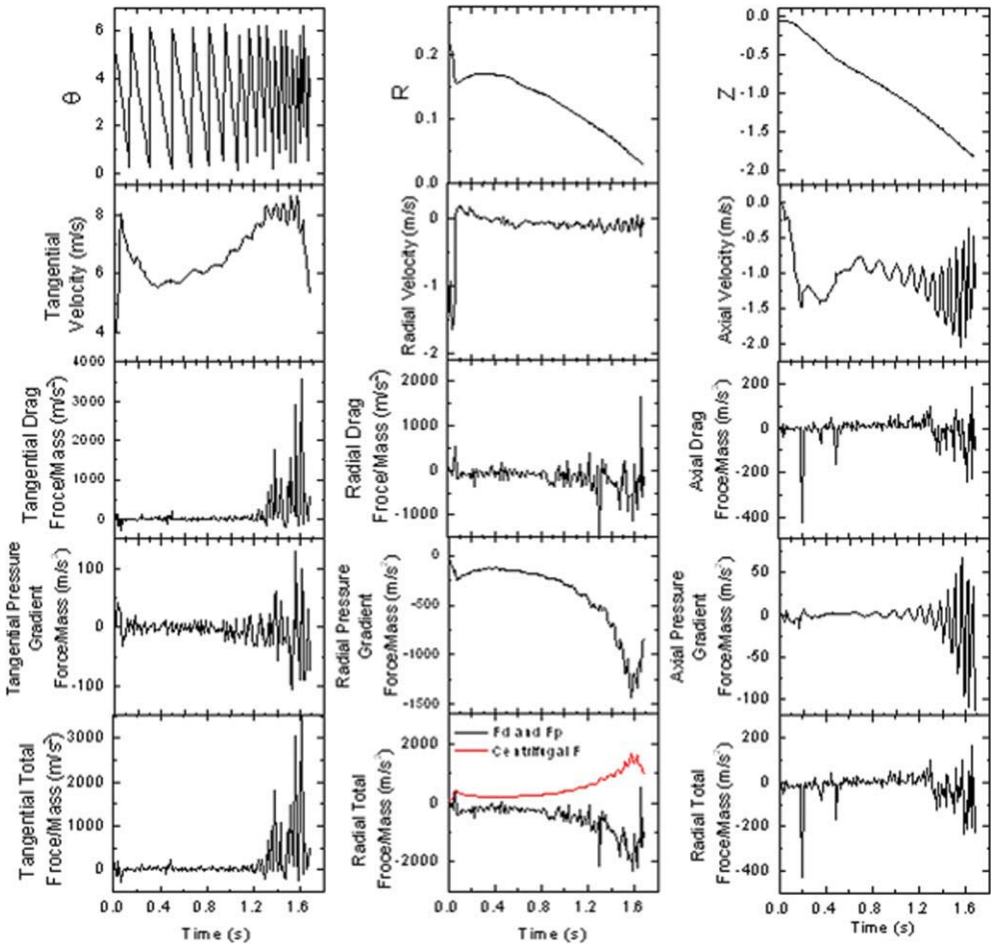

Figure 6. Dynamic result of a representative 46 μm particle (columns: tangential, radial, and axial directions; rows: position, velocity, drag force, pressure gradient force, and total force).

[Color figure can be viewed in the online issue, which is available at www.interscience.wiley.com.]

separation region of 31 μm particles is broader than that of 46 μm particles. Because of the contracting LZVV size, the moving orbit of 31 μm particles is wider. Second, as particle size decreases, the effect of the drag force becomes significant. The position of fine particles would fluctuate stochastically in the radial direction.

Flow of particles in Region C (dip point vs. critical point)

As shown in Figure 3, Region C is bound by the dip point and the critical point. So, it is interesting to investigate the behavior of particles at the two points. As shown in Figure 8, 16 μm particles which have the smallest separation efficiency show a similar dynamic behavior to 31 μm particle. The effect of the drag force becomes more intensive than that of the coarser particles in the radial direction. Therefore, the particles have a high probability to pass the LZVV and move upward, resulting in a low underflow.

From Figure 5d, it can be seen that the separation region is large, from the cylindrical part to the bottom of the cyclone. Correspondingly, the moving orbit of upward particles is wider than the coarser particles analyzed earlier. Some particles even move to the area between the walls of the vortex finder and the cyclone body. In this case, the particles are collected by the short circuit flow and report to the overflow, resulting in a low separation efficiency.

Particles in Region C behavior differently from those in Region B. As a typical example, the flow of particles at the critical point is analyzed. From the first row of Figure 9, it can be seen that the 1 μm particle goes down first. At 1.2 s when the particle flows in the cylinder, it passes the LZVV and moves up with the upward flow. According to the plot of the Z and R positions, it travels to the area between the outside wall of vortex finder and the inside wall of cyclone body and stays there for a long time. At 4 s, this particle is captured by the main downward flow again and reports to the underflow finally. The total residence time is about 6 s. The fluctuation of the velocity is huge due to the effect of the huge drag force. The pressure gradient force remains at a low level at the same conditions. In other words, this fine particle has a strong stochastic characteristic.

Figure 5e shows that the separation of 1 μm particles could happen anywhere, since the fluctuating velocity is very

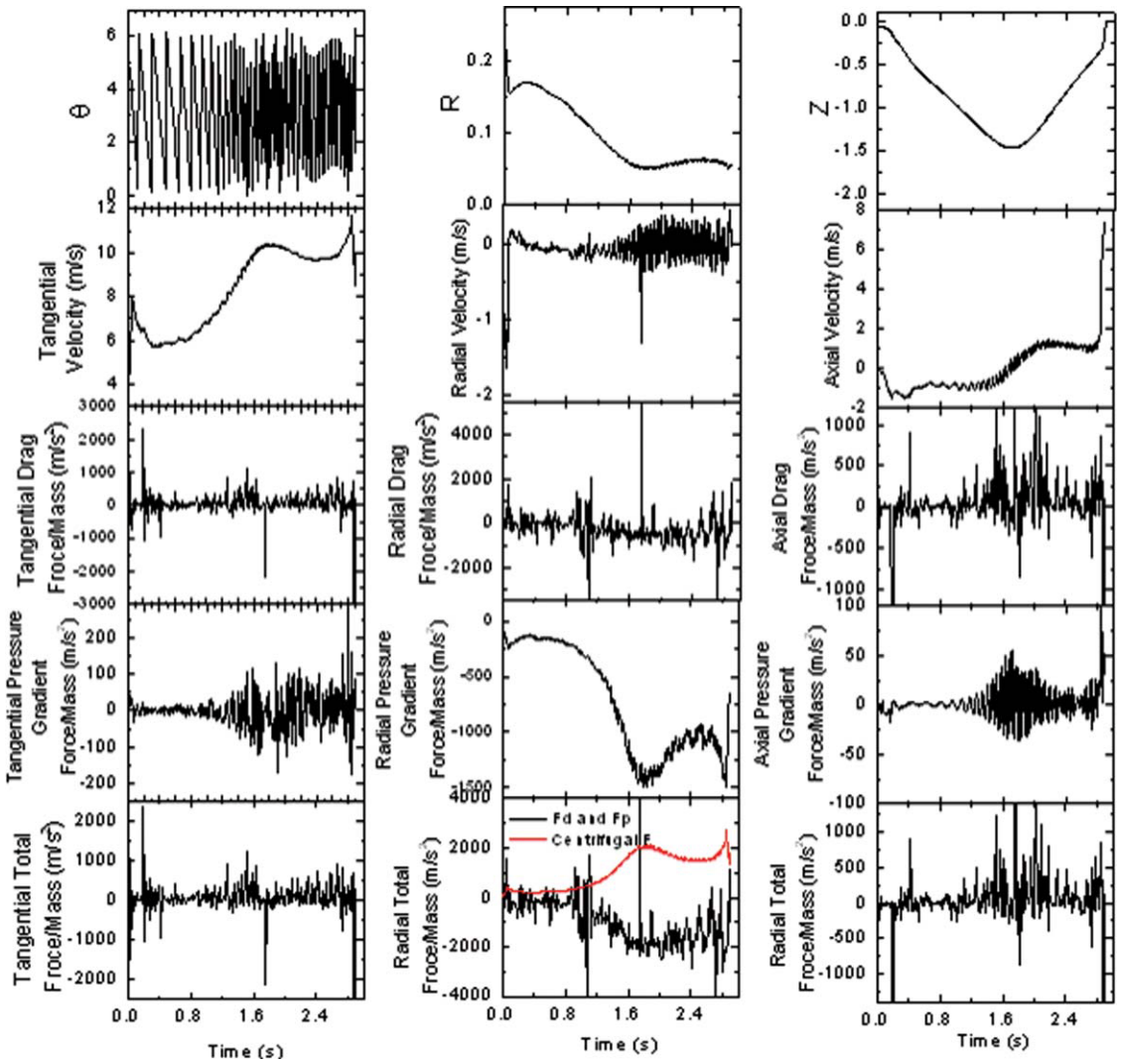

Figure 7. Dynamic result of a representative 31 μm particle (columns: tangential, radial, and axial directions; rows: position, velocity, drag force, pressure gradient force, and total force).

[Color figure can be viewed in the online issue, which is available at www.interscience.wiley.com.]

significant. Also the moving orbit of such a particle could be much wider due to the effect of the drag force. The boundary of the moving orbit can even reach the LZVV. In particular, some upward particles could go to the downward flow. In this way, the particles would recircuit between the upward and downward flows, which was observed by Cullivan et al.[26] and get more chances to separate again. This results in a high separation efficiency and hence the fish-hook phenomenon.

Role of the forces in different regions

To better understand the mechanisms governing the particle separation and fish-hook phenomenon, the forces controlling the motion of particles are further analyzed. According to Eq. 1, the motion of a particle is governed by the pressure gradient force, the drag force and the gravity force. It is noted that the centrifugal force largely represents the motion of particles in the tangential direction, resulting from the inlet and cyclone settings but not an active force as given in Eq. 1. Figure 10 shows the magnitudes of the three forces in the radial direction, which are the pressure gradient force, centrifugal force and drag force. The pressure gradient force always points inward and the centrifugal force points outward in the radial direction. But the drag force shows a strong stochastic characteristic and its direction depends on the relative velocity between particle and fluid. It can be seen from the figure that as particle size decreases, the pressure gradient force and the centrifugal force do not change much. Generally, the magnitudes of the two forces are close. They form a force balance on a particle in the radial direction. For the hydroclone considered, for all particles, the centrifugal force is slightly larger than the pressure gradient force, which will keep particles staying in the downward flow near the wall. As particle size decreases, the drag force, which includes the turbulent effect as implied by Eq. 3, has

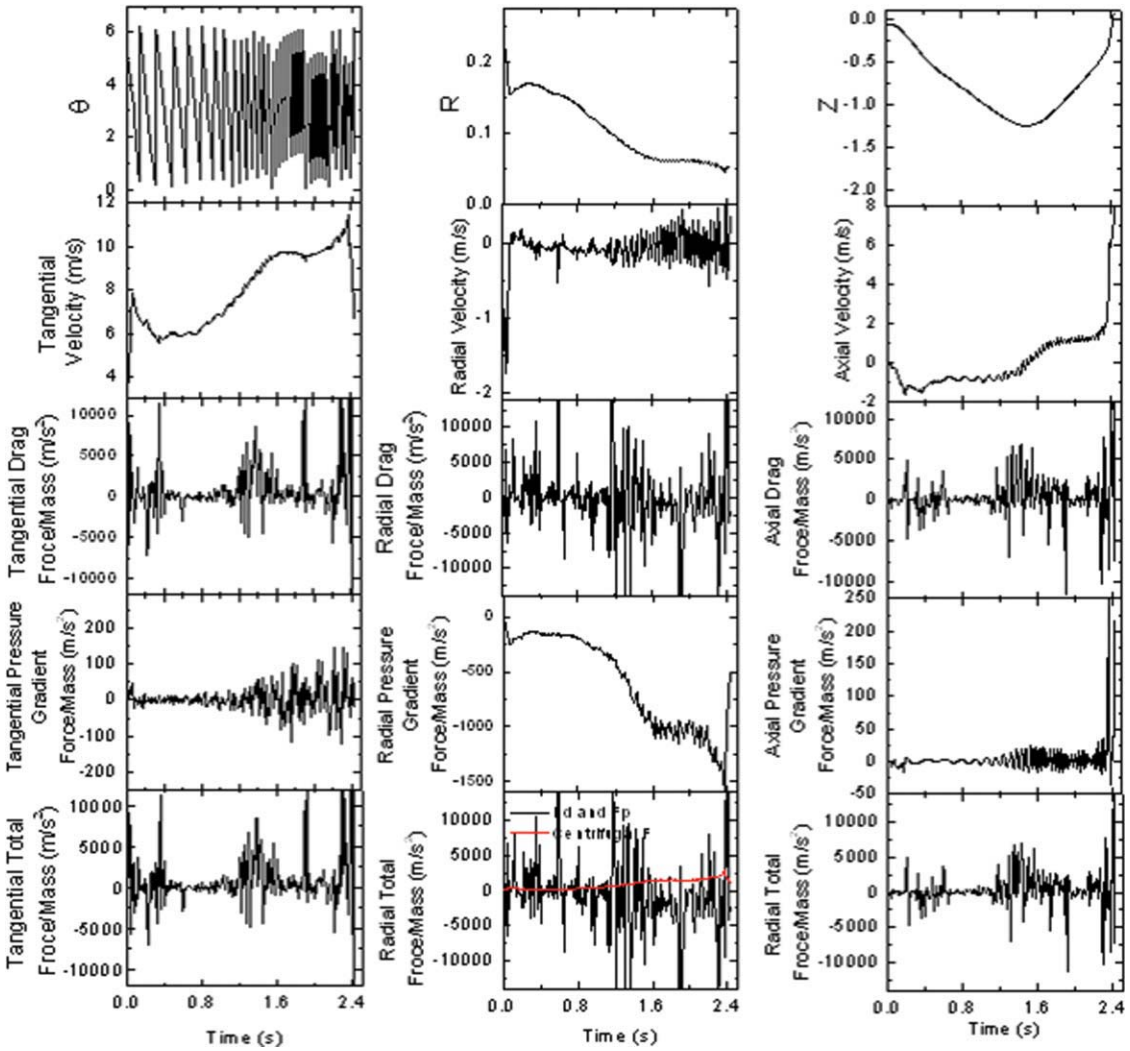

Figure 8. Spatial distribution of 16 μm particles (columns: tangential, radial, and axial directions; rows: position, velocity, drag force, pressure gradient force, and total force).

[Color figure can be viewed in the online issue, which is available at www.interscience.wiley.com.]

an exponential growth and its direction is stochastic. This force plays an interesting role in particle separation.

For coarse particles in Region A with 100% separation efficiency to the underflow, the stochastic drag force is too small to destroy the balance formed by the centrifugal force and the pressure gradient force. In this case, coarse particles stay in the downward flow and report to the spigot. For mid-size particles in Region B with the lowest to 100% efficiency shown in Figure 3, normally, the drag force is too small in the cylindrical part to break the balance, so the particles follow the downward flow. When the particles enter the conical part near the spigot, where the turbulence intensity is high, the stochastic drag force becomes large and as a result, they have more fluctuation at their position. Therefore, the particles have more opportunities to cross the LZVV and join the upward flow. It is noted that since such kind of particles go into the upward flow stochastically, the probability to the overflow never reaches 100%. When some particles stay in the upward flow, where the turbulence intensity is relatively small, the particles have a certain moving orbit in the inner flow. As particle size decreases, the effect of the drag force increases and the region where the particles turn around becomes large. Because of the contracting LZVV size and the fluctuating velocity of particles, the moving orbit in the upward flow becomes wide.

For ultrafine particles in Region C, the effect of the drag force is very strong and much larger than the centrifugal force and the pressure gradient force. Therefore, such fine particles can pass the LZVV with a high probability and the moving orbit in the upward flow is very wide. Some particles can be pushed to the downward flow again by the drag force and get one more chance to go to the spigot, resulting in a high separation efficiency to the underflow. The smaller the particles, the more significant is the effect. As a result, the partition curve looks like a fish-hook.

Effects of other variables

It is known that the aforementioned governing forces and hence the flow of particles are affected by many variables

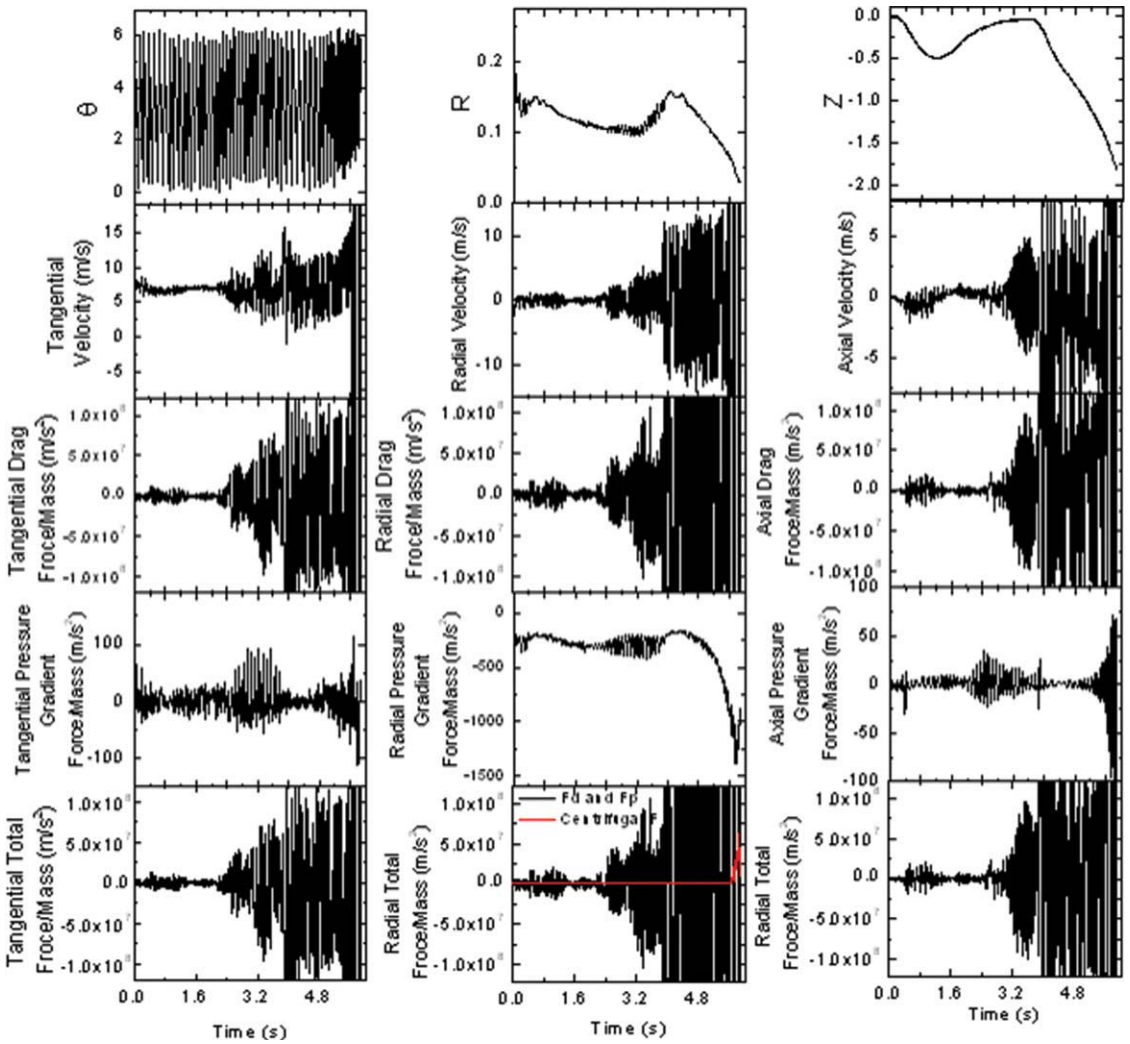

Figure 9. Dynamic result of a representative 1 μm particle (columns: tangential, radial, and axial directions; rows: position, velocity, drag force, pressure gradient force and total force).

[Color figure can be viewed in the online issue, which is available at www.interscience.wiley.com.]

related to the cyclone geometry, material properties, and operational conditions. It would be of interest to examine if the change of any of such variables affects the aforementioned findings. This will need a systematic study that is far beyond the current research effort. Nonetheless, numerical experiments have been extended to investigate the effects of two key variables, namely cyclone size and liquid viscosity. This is done by varying cyclone size or liquid viscosity while all the other parameters are the same as used earlier. When the cyclone size changes, all the variables related to the cyclone geometry change in the same proportion.

Figure 11 shows the effect of cyclone size on the partition curve. Obviously, the fish-hook effect can be observed for all the sized cyclones considered. As the body diameter increases, the recovery efficiency at the dip point decreases. The main reason could be that the bigger the cyclone diameter, the smaller the fluid split ratio reported to the underflow.[22] That is, the fluid flow rate at the underflow decreases with the cyclone size. In a small hydrocyclone, more particles of sizes around the dip point are carried by the fluid and report to the underflow, which results in an increased recovery efficiency for these particles. Moreover, the range of Region C increases with the cyclone size. These results could be explained from the changed orbit radius of the LZVV region. As the body diameter increases, the orbit radius increases. Consequently, the probability for particles to pass LZVV decreases, resulting in an extended Region C for relatively large cyclones.

Figure 12 shows the effect of liquid viscosity on the fish hook phenomenon. Note that in this work, the liquid is assumed to be homogeneous with a single viscosity and density. As the viscosity increases, the recovery efficiency in Region B decreases but that in Region C decreases. Moreover, the particle size at the dip point and the recovery efficiency at this point increase. The decreased recovery efficiency corresponds to the fact that the split ratio is small with a low fluid viscosity. Figure 13 shows the spatial distribution of turbulence intensity for different liquid viscosities. As the liquid viscosity increases, the turbulence intensity increases, particularly in the conical part. Consequently,

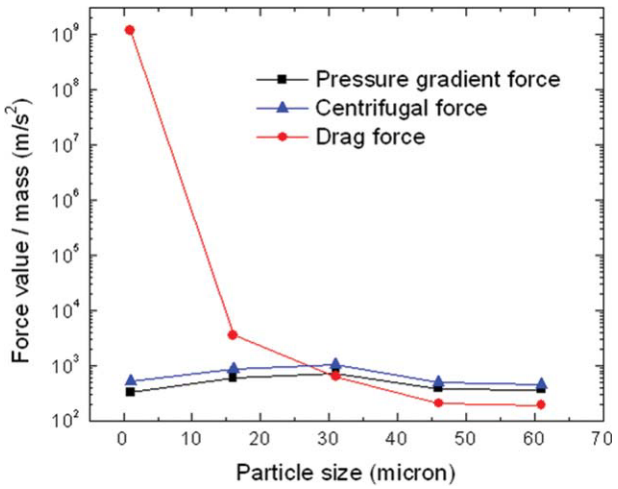

Figure 10. Simulated results of normalized average forces in the radial direction as a function of particle size.

[Color figure can be viewed in the online issue, which is available at www.interscience.wiley.com.]

more particles have fluctuating velocities and obtain a higher probability to pass the LZVV, resulting in a low recovery efficiency. When these particles move to the cylindrical part, they also have a high probability to pass the LZVV again, producing an increased dip point.

The results in Figures 11 and 12 suggest that changing the cyclone size and liquid viscosity will change the partition curve for a given system. However, the mechanisms identified earlier are still valid. Therefore, it is important to understand the flow of particles and the governing forces, although the fish-hook phenomenon may be multifaced, As mentioned earlier, there are many variables involved, which are related to the cyclone geometry, material properties and operational conditions. Further work is necessary in order to understand the fish-hook phenomenon in relation to these variables.

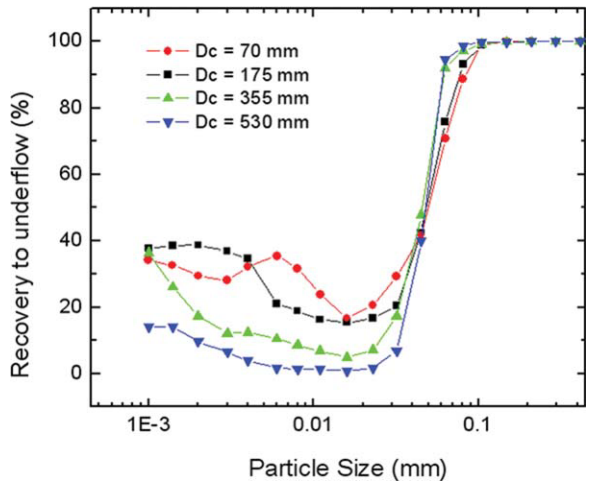

Figure 11. The partition curves of the hydrocyclones of different body sizes.

[Color figure can be viewed in the online issue, which is available at www.interscience.wiley.com.]

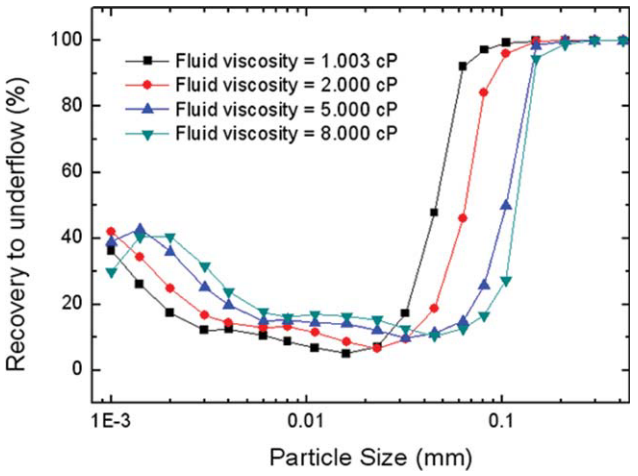

Figure 12. The partition curve of the hydrocyclones, operated with liquids of different viscosities.

[Color figure can be viewed in the online issue, which is available at www.interscience.wiley.com.]

Conclusions

A computer model has been developed to reproduce the particle separation and fish-hook phenomenon in a hydrocyclone. The model includes the RSM to describe the anisotropic turbulence flow, VOF to determine the interface between air and fluid, and a stochastic Lagrangian model to predict the flow of particles. Numerical investigation has been carried out on the dynamics of particles in relation to the mechanisms of separation and fish-hook phenomenon. The following conclusions can be drawn.

The motion of a particle in a hydrocyclone is governed by a range of particle-fluid and particle-wall interaction forces. There are three main forces that should be considered for the dilute system considered in this work, namely, the fluid drag force, pressure gradient force, and centrifugal force, in

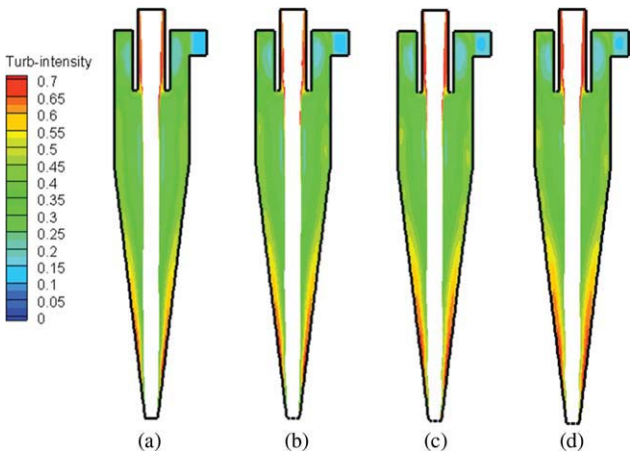

Figure 13. Spatial distribution of turbulence intensity in the hydrocyclones, operated with liquids of different viscosity.

(a) liquid viscosity = 1.003 cP, (b) liquid viscosity = 2.000 cP, (c) liquid viscosity = 5.000 cP, and (d) liquid viscosity = 8.000 cP. [Color figure can be viewed in the online issue, which is available at www.interscience.wiley.com.]

addition to the gravity force. The drag force is directly related to the fluid flow which is mainly downward outside the LZVV and upward within the LZVV while maintaining its tangential flow introduced at the inlet. The force plays a dominant role on the particle motion in the tangential and axial directions. In the radial direction, however, the pressure gradient force is the driving force to make particles move inward, which is missed in almost all the previous studies. It balances the centrifugal force in controlling the motion of particles, particularly for coarse particles. But the drag force induces a fluctuating velocity which makes the motion of particles stochastic, particularly for fine particles and near the spigot where the turbulence intensity is high. The complicated motion of particles in a hydrocyclone results from the collective outcome of these forces.

In a normal operation, the centrifugal force on a particle is usually larger than the pressure gradient force so that liquid and solids can separate. However, as particle size decreases, the drag force increases sharply, which results in different behaviors of particles of different sizes. Coarse particles (in Region A) will flow outside the LZVV and report to the underflow because the effect of the drag force is small. Medium particles (in Region B), driven by the fluctuating drag force, may break the balance of the pressure gradient force and the centrifugal force to pass the LZVV, join the upward flow and report to the overflow. The smaller the particle size, the more particles report to the overflow, hence lower recovery to underflow. However, fine particles (in Region C) behavior differently, because the drag force is more significant and can cause a wider orbit radius in the upward flow even beyond the LZVV and recircuit between the downward and upward flows. This will result in relatively high separation efficiency and the fish-hook effect.

The effects of cyclone size and liquid viscosity have also been examined. The results suggest that the mechanistic understanding developed in this work may be general, although further work is necessary in order to comprehensively understand the fish-hook phenomenon in relation to many variables related to cyclone geometry, material properties and operational conditions.

Acknowledgments

The authors thank the Australian Research Council for the financial support of this work.

Literature Cited

1. Bradley D. *The Hydrocyclone*. London: Pergamon, 1965.
2. Svarovsky L. *Hydrocyclones*. Lancaster, PA: Technomic Publishing, 1984.
3. Frachon M, Cilliers JJ. A general model for hydrocyclone partition curves. *Chem Eng J*. 1999;73:53–59.
4. Majumder AK, Shah H, Shukla P, Barnwal JP. Effect of operating variables on shape of "fish-hook" curves in cyclones. *Miner Eng*. 2007;20:204–206.
5. Plitt LR. A mathematical model of the hydrocyclone classifier. *CIM Bull*. 1976;69:114–123.
6. Flintoff BC, Plitt LR, Turak AA. Cyclone Modeling—a review of present technology. *CIM Bull Sep*. 1987;80:39–50.
7. Nageswararao K. A critical analysis of the fish hook effect in hydrocyclone classifiers. *Chem Eng J*. 2000;80:251–256.
8. Roldán-Villasana EJ, Williams RA, Dyakowski T. The origin of the fish-hook effect in hydrocyclone separators. *Powder Technol*. 1993;77:243–250.
9. Finch JA. Modelling a fish-hook in hydrocyclone selectivity curves. *Powder Technol*. 1983;36:127–129.
10. Neesse T, Dueck J, Minkov L. Separation of finest particles in hydrocyclones. *Miner Eng*. 2004;17:689–696.
11. Kraipech W, Chen W, Parma FJ, Dyakowski T. Modelling the fish-hook effect of the flow within hydrocyclones. *Int J Miner Process*. 2002;66:49–65.
12. Majumder AK, Yerriswamy P, Barnwal JP. The "fish-hook" phenomenon in centrifugal separation of fine particles. *Miner Eng*. 2003;16:1005–1007.
13. Hsieh KT, Rajamani RK. Mathematical-model of the hydrocyclone based on physics of fluid flow. *AlChE J*. 1991;37:735–746.
14. Monredon TC, Hsieh KT, Rajamani RK. Fluid-flow model of the hydrocyclone—an investigation of device dimensions. *Int J Miner Process*. 1992;35:65–83.
15. Nowakowski AF, Cullivan JC, Williams RA, Dyakowski T. Application of CFD to modelling of the flow in hydrocyclones. Is this a realizable option or still a research challenge? *Miner Eng*. 2004;17:661–669.
16. Martinez LF, Lavin AG, Mahamud MM, Bueno JL. Vortex finder optimum length in hydrocyclone separation. *Chem Eng Process*. 2008;47:192–199.
17. Hwang KJ, Hsueh WS, Nagase Y. Mechanism of particle separation in small hydrocyclone. *Dry Technol*. 2008;26:1002–1010.
18. Wang B, Chu KW, Yu AB. Numerical study of particle-fluid flow in a hydrocyclone. *Ind Eng Chem Res*. 2007;46:4695–4705.
19. Bergstrom J, Vomhoff H. Experimental hydrocyclone flow field studies. *Sep Purif Technol*. 2007;53:8–20.
20. Hsieh KT. Phenomenological model of the hydrocyclone, PhD Thesis, The University of Utah, USA, 1988.
21. Wang B, Chu KW, Yu AB, Vince A. Modeling the multiphase flow in a dense medium cyclone. *Ind Eng Chem Res*. 2009;48:3628–3639.
22. Wang B, Yu AB. Numerical study of particle-fluid flow in hydrocyclones with different body dimensions. *Miner Eng*. 2006;19:1022–1033.
23. Wang Z-B, Chu L-Y, Chen W-M, Wang S-G. Experimental investigation of the motion trajectory of solid particles inside the hydrocyclone by a Lagrange method. *Chem Eng J*. 2008;138:1–9.
24. Kallio GA, Reeks MW. A numerical simulation of particle deposition in turbulent boundary layers. *Int J Multiphase Flow*. 1989;15:433–446.
25. Tabor D, Winterto Rh. The direct measurement of normal and retarded van der Waals forces. *Proc R Soc Lond Ser Math Phys Sci*. 1969;312:435–450.
26. Cullivan JC, Williams RA, Cross CR. Understanding the hydrocyclone separator through computational fluid dynamics. *Chem Eng Res Des*. 2003;81:455–466.

Manuscript received Apr. 6, 2009, and revision received Sept. 8, 2009.